# U-Net based Multi-level Texture Suppression for Vessel Segmentation in Low Contrast Regions

Kamini Upadhyay[1], Monika Agrawal[2], and Praveen Vashist[3]

[1,2]Centre for Applied Research in Electronics, IIT Delhi, New Delhi, India
[3]Community Ophthalmology, AIIMS Delhi, New Delhi, India
Email ids: [1]kaminiup23@gmail.com, [2]maggarwal@care.iitd.ac.in, [3]praveenvashist@yahoo.com

***Abstract*—Segmentation of retinal blood vessels is important for diagnosis of many retinal diseases. Precise segmentation of complete vessel-map is still a challenge in low contrast regions of fundus images. Vessel pixels belonging to these regions, such as, fine vessel-endings and boundaries of vessels, get merged in the neighboring vessel-like texture. This paper proposes a novel retinal vessel segmentation algorithm which handles the background vessel-like texture in a sophisticated manner without harming the vessel pixels. In this work, first we enhance all possible vessel-like features of fundus at different 'levels' using 2-D Gabor wavelet and Gaussian matched filtering. At each 'level', texture is suppressed using Local Laplacian filter while preserving the vessel edges. The resulting images are combined to produce a maximum response image with enhanced vessels of different thicknesses and suppressed texture. This handcrafted image is used to train the deep U-net model for further suppression of non-vessel pixels. Proposed segmentation method is tested on publicly available DRIVE and STARE databases. The algorithm has produced state-of-the-art results. It has performed outstandingly well in terms of sensitivity measure which is most affected with the correct segmentation of fine vessels and vessel-boundary pixels present in low-contrast regions.**

***Index Terms*—segmentation, texture suppression, multiscale, U-net.**

## I. Introduction

Medical image analysis has emerged as an inevitable step in the field of diagnostics. Recent improvements in the quality of image acquisition, high speed device-to-device transfer of acquired images, very high data storage capacity and extremely high computational efficiency are some factors that have helped in making the process of automated diagnosis of diseases more precise. Feature localization and their segmentation, constitute the core of medical image analysis.

Retinal image analysis has been very helpful in diagnosis of many retinal diseases like Diabetic Retinopathy (DR), Glaucoma, Age-related Macular Degeneration (AMD) etc. Digital fundus images have provided us an efficient way to capture 2-D projection of retina. In case of retina, blood vessels enter through the Optic Disc (OD) and spread in Y-shaped pattern, with continuously decreasing thickness. Retina and its features can be analysed with the help of fundus images. In a color fundus, OD can be seen as a bright-yellow disc and vessels appear as dark tubular structures originating from OD and spreading across the retina. Vessel thickness keeps decreasing with the spreading, which leads to thin vessel-ends which are poorly-illuminated and in poor contrast with respect to the retinal non-vessel background. The main challenge while segmenting retinal blood vessels is, the 'completeness' of vessel map. Low-contrast regions of fundus image disturb the process of precise vessel segmentation and lead us to many false positives and false negatives.

Researchers are exploring each possible direction to segment retinal vessel map. Various conventional rule-based methods include filter based methods [3], [8], [12]; matting based [1]; multiscale based [11], [17]; active contour based [16] etc. Machine learning has been used with various possible features corresponding to blood vessels. Neural Networks [14], Gaussian Mixture Model [11] etc. are used to classify the image pixels as vessel or non-vessel. With the advancements in data-handling, deep learning (DL) based segmentation methods are also being proposed. Liskwoski et al. [7] trained a deep neural network for vessel segmentation. Yan et al. [2] proposed a DL based method to manage pixel imbalance between thick and thin vessels. U-net model [4] and its variants [5] have been proposed, specifically, to handle segmentation in medical images. Jiang et al. [18] proposed a multi-scale information fusion module to extract retinal vessels of different thicknesses.

Retinal blood vessel segmentation is still an active area of research. Even in case of a healthy retina, precise segmentation of vessels is difficult. Less sharp boundaries of vessels and poorly-contrasted thin vessels are some difficult portions of fundus images. Extraction of thin-to-thick retinal vessel map, which includes the complete thickness of major vessels alongwith the fine vessels, is a challenge. This paper proposes a novel vessel segmentation algorithm which resolves the problem of segmentation in low-contrast regions. These regions have vessel and background pixels of similar intensity values, which are almost inseparable. This algorithm separates these pixels at mutiple 'levels'. It first enhances all the vessel-like features and then vessel-like background texture is suppressed while preserving the strong vessel edges, at different levels. These preserved edges at different levels are combined by extracting the maximum value at each pixel. This handcrafted feature image is used to train U-net based model [4], which gives the final segmented vessel map.

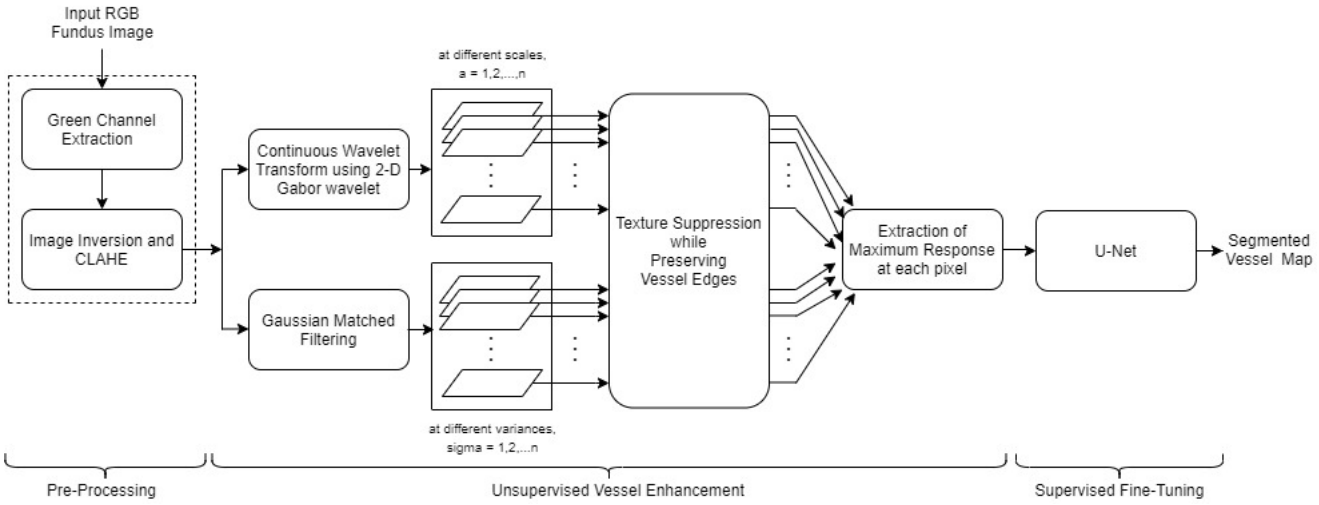


Fig. 1: *Block diagram of the proposed algorithm.*

## II. Proposed Method

Vessel segmentation methods, generally, fail in regions of poor-contrast. Here, vessels merge in the background vessel-like texture. It badly affects the performance of algorithm and leads into high false positive rate in the end. Proposed method works in three stages, 1. Pre-processing, 2. Unsupervised vessel enhancement and 3. Supervised fine tuning. Fig. 1 presents block diagram representation of the proposed method.

### A. Pre-processing

To prepare the input color fundus image for the proposed algorithm, some simple pre-processing steps are applied. We assume $\{I(x,y)|x,y \in \mathbb{Z}\}$ to be the input color fundus image shown in Fig. 2 (a). It is observed that the green channel of fundus images has the best contrast between vessels and background [8]. Thus, we extract the green channel $I_g(x,y)$ of input fundus, shown in Fig. 2 (b). This image is inverted and contrast-enhanced using contrast limited adaptive histogram equalization (CLAHE) [6]. The image $I_{CLAHE}(x,y)$ is now ready for further processing shown in Fig. 2 (c).

### B. Unsupervised Vessel Enhancement

This is the core step of our proposed algorithm. It includes 2-D Gabor Wavelet Analysis at multiple scales ($a$) and Gaussian Matched filtering at multiple spreads ($\sigma$). We will use the term 'level', throughout the paper, to combinely denote different values of $a$ and $\sigma$. The resulting images at each 'level' are processed using Local Laplacian filter. In the end, out of mutli-level responses for each pixel, maximum response value is retained.

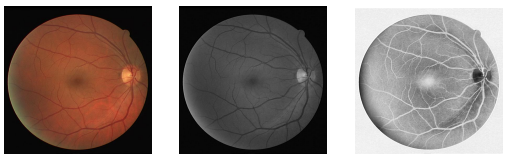

(a) (b) (c)

Fig. 2: Illustration of Pre-processing stage : (a) Input RGB fundus image '19_test' from DRIVE dataset, (b) Extracted green channel, (c) Inverted and contrast enhanced green channel.

*1) 2-D Gabor Wavelet Analysis:* In wavelet analysis, the mother wavelet is choosen according to the feature of interest. Our interest, blood vessels, can be seen as directional edges present in retinal images with cross-sectional Gaussian intensity profile [8]. Here, Gabor wavelet, which is a complex modulated Gaussian, is used [11] for vessel enhancement.

Let $\psi(\mathbf{x})$ denotes the 2-D Gabor wavelet, given as,

$$\psi(\mathbf{x}) = \exp(j\mathbf{k_0}\mathbf{x}) \exp\left(-\frac{1}{2}|A\mathbf{x}|^2\right) \tag{1}$$

where $\mathbf{x} \in \mathbb{R}^2$, $\mathbf{k_0}$ is the wave vector defining the frequency of complex exponential, $A = \text{diag}[\epsilon^{-1/2}, 1]$ is a 2x2 positive definite matrix, with $\epsilon \geq 1$ making the function anisotropic.

A family of wavelets $\psi_{\mathbf{b},\theta,a}(x,y)$ can be defined by translations ($\mathbf{b}$), rotations ($\theta$) and dilations ($a$) of the analyzing wavelet $\psi(x,y)$. For each image, the continuous wavelet transform (CWT), $I^{\psi}(x,y,\theta,a)$, is defined in terms of the scalar product $\langle \cdot,\cdot \rangle$ of $I_{CLAHE}(x,y)$ with the transformed analyzing wavelet $\psi_{\mathbf{b},\theta,a}(x,y)$,

$$I^{\psi}(x,y,\theta,a) = C_{\psi}^{-1/2} \langle \psi_{\mathbf{b},\theta,a}(x,y), I_{CLAHE}(x,y) \rangle, \forall (x,y) \tag{2}$$

where, $C_{\psi}$, $\psi$, $\mathbf{b}$, $\theta$ and $a$ denote the normalizing constant, analyzing wavelet, displacement vector, rotation angle, and scale parameter (or dilation parameter), respectively. We observe that the absolute of the real coefficients maximized over all the orientations, give the best vessel response. Thus we denote these coefficients as $R_a(x,y)$ at scale $a$ and define them as,

$$R_a(x,y) = \Big| \max_{\theta} \left[ Re\{I^{\psi}(x,y,\theta,a)\} \right] \Big|, \forall (x,y) \tag{3}$$

Different scale values $a$, helps in enhancing oriented vessels of different thicknesses. Along-with the vessels, texture of the

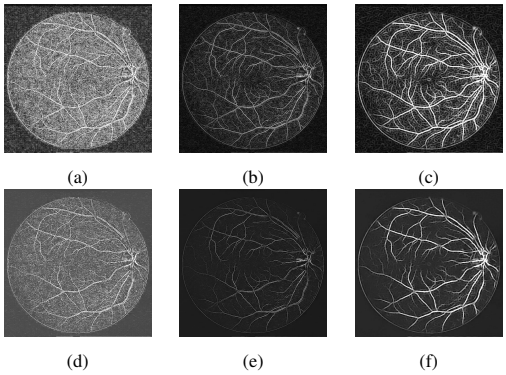

Fig. 3: Vessel Enhancement using Gabor Wavelet at different scales : (a) $a$=1 , (b) $a$=2 (c) $a$=3; Texture Removal at different scales : (d) $a$=1, (e) $a$=2, (f) $a$=3

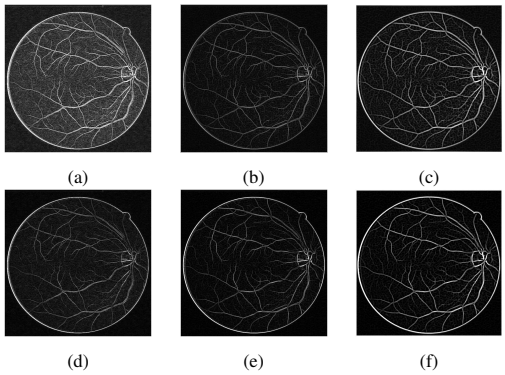

Fig. 4: Gaussian Matched Filtering at different spreads : (a) $\sigma$=1 , (b) $\sigma$=2 (c) $\sigma$=3; Corresponding Texture Removal at each variance : (d) $\sigma$=1 , (e) $\sigma$=2 (f) $\sigma$=3

background with similar intensity-profile is also enhanced. Fig. 3 (a), (b) and (c) denote the vessel enhanced images corresponding to scale values $a$=1, 2 and 3, respectively, used in the proposed work.

*2) Gaussian Matched Filtering:* In previous section, we assumed cross-sectional vessel intensity profile to be Gaussian. In this section, with the same assumption we apply Gaussian shaped 2-D rotating kernels to the pre-processed fundus image $I_{CLAHE}(x, y)$. A 2-D Gaussian kernel is defined as [8],

$$K_\sigma(x, y) = \frac{1}{\sigma\sqrt{2\pi}} exp(-\frac{x^2}{2\sigma^2}) \forall |x| \leq 3\sigma, |y| \leq L/2 \quad (4)$$

Here, $L$ denotes the length of kernel for which the vessel is assumed to have fixed orientation, $\sigma$ denotes the spread of Gaussian curve which covers the thickness of vessel. This kernel assumes vessel-length along y-axis and its spread (thickness) along x-axis ($\pm 3\sigma$). Positive values of kernel denote that in our algorithm after pre-processing vessels are brighter than background.

In this work, we have generated multiple Gaussian kernels corresponding to different values of $\sigma$ for different vessel thicknesses. Each kernel is rotated at angle $\theta$ covering all possible orientations from 0°-180°. $K^\theta_\sigma(x, y)$ denotes a 2-D Gaussian kernel with spread $\sigma$, tilted at orientation $\theta$,

$$K^\theta_\sigma(x, y) = Rot_\theta\{K_\sigma(x, y)\}, \forall (x, y) \quad (5)$$

Here, $Rot_\theta\{.\}$ denotes the operator which rotates the input kernel by angle $\theta$ in anti-clockwise direction. For a particular value of $\sigma$, this kernel is matched with the pre-processed image $I_{CLAHE}(x, y)$ at all orientations $\theta$. The maximum response over all the angles is retained in $G_\sigma(x, y)$ as,

$$G_\sigma(x, y) = \max_\theta [MFR\{I_{CLAHE}(x, y), K^\theta_\sigma(x, y)\}], \forall (x, y) \quad (6)$$

Here, $MFR\{.\}$ denotes the matched filtering operator which matches the rotating 2-D kernel with the pre-processed image. Different values of spreads $\sigma$, help in enhancing oriented vessels of different thicknesses. Along-with these vessels, texture of the background with similar intensity-profile is also enhanced. Fig. 4 (a), (b) and (c) denote the vessel enhanced images corresponding to spread values $\sigma$=1, 2 and 3, respectively, used in the proposed work.

*3) Texture Suppression while Preserving Vessel Edges:* At this stage, we have multiple responses at different 'levels' corresponding to different values of $a$ and $\sigma$. These images have enhanced vessels along-with many vessel-like background texture. Now, we apply edge-preserving, Local Laplacian filter [10] to suppress this vessel-like texture at each 'level'.

Local Laplacian Filter (LLF) decomposes the input image into its corresponding Gaussian pyramids. For each pixel value in the pyramid, the input image is remapped using a point-wise function to build a Laplacian pyramid. For our purpose, an 'S-shaped' transformation is used to boost the vessel pixels and suppress the non-vessel pixels. This process is repeated for each pixel over all the decomposition until the output pyramid is filled to give the final response. This helps in suppressing fine vessel-like texture while preserving the strong vessel edges. Let $LLF\{.\}$ denotes the Local Laplacian Filter operator, $S_a(x, y)$ and $S_\sigma(x, y)$ denote the texture-smoothened output images at each level then,

$$S_a(x, y) = LLF\{R_a(x, y)\}, \forall (x, y) \quad (7)$$

$$S_\sigma(x, y) = LLF\{G_\sigma(x, y)\}, \forall (x, y) \quad (8)$$

Fig.3 (d), (e) and (f) show the resulting images after texture suppression at different scales $a$=1, 2 and 3, respectively. Similarly, Fig. 4 (d), (e) and (f) present the images after texture suppression at $\sigma$=1, 2 and 3, respectively.

The resulting smooth images at all the levels are combined by retaining the maximum value at each pixel $(x, y)$ as $M(x, y)$ i.e.,

$$M(x, y) = max\{S_a(x, y), S_\sigma(x, y)\}, \forall (x, y) \quad (9)$$

This maximum response corresponding to image '19_test' is shown in Fig. 5 (b).

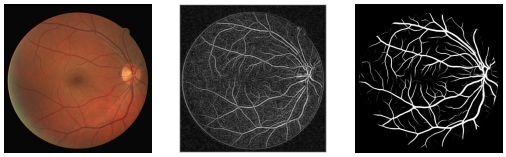

(a) (b) (c)

Fig. 5: (a) Input color fundus image '19_test' from DRIVE dataset , (b) Maximum response image with suppressed local texture $M(x, y)$, (c) Extracted gray-scale vessel map using U-net.

### C. Supervised Fine-Tuning

At this stage, we have an exhaustively enhanced image with suppressed texture. We feed this image to train a DL based classifier called U-net to fine tune our segmentation process. U-net model is a symmetric, contracting-expanding deep learning model, specifically developed for segmentation of medical images [4]. It has convolution layers followed by ReLU activation layer, max pooling layers and up-sampling layers. High-resolution information is passed, directly, from contracting path to expanding path. This architecture is developed in such a manner that it is very good at capturing image context along-with a precise localization.

Researchers have used the same model or its modifications using RGB fundus images [4], [5]. Training this model with a handcrafted, unsupervised vessel enhanced image leads into much better performance of this model. The fine vessels and the vessel boundary pixels are already enhanced, which will help in the model learning at these low-contrast, challenging regions.

For training, we use 7000 patches per image, of height and width $48 \times 48$. The patches are chosen randomly. A total of 140000 patches for 20 training images from DRIVE [13] data-set are generated. This patch-based training resolves the issue of scarcity of annotated data in case of bio-medical images, upto some extent. We have not used any kind of data augmentation in this work. 90% of the total patches are used for training and rest 10% are used for validation purpose. We define cross entropy as our loss function and the optimizer used to minimize this loss is Stochastic Gradient Descent (SGD).

## III. Material and Results

Proposed algorithm is developed using DRIVE [13] and STARE [12] databases, available on public domain. DRIVE has 40 color fundus images of dimension $584 \times 565$. Images are annotated by two experts. STARE database has 20 color fundus images of size $605 \times 700$ annotated by two experts. We have used the images from 'training set' of DRIVE data-set for training the model and testing is performed on test-set of DRIVE and complete STARE data-set. Annotations done by Expert-1 are used to measure the performances.

In this paper, for evaluating the performance of proposed algorithm we have used eight metrics namely, Accuracy ($Acc$), Sensitivity ($Sen$), Specificity ($Spe$), Precision ($Pr$), F1-score ($F1$), G-mean ($G$), Matthews Correlation Coefficient ($MCC$)

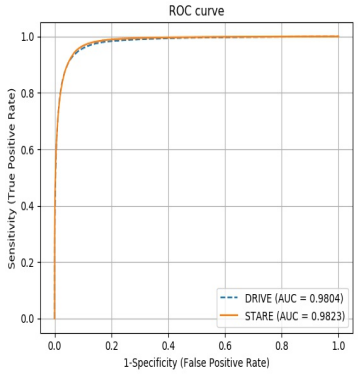


Fig. 6: *Mean ROC curve obtained for DRIVE and STARE data-sets*

and Area under Receiver Operating Characteristics Curve ($AUC$-$ROC$). Mathematical definitions of these measures are given below,

$$Acc = \frac{(TP+TN)}{(TP+TN+FP+FN)}; Sen = \frac{(TP)}{(TP+FN)}$$

$$Spe = \frac{(TN)}{(TN+FP)}; Pr = \frac{(TP)}{(TP+FP)}; G = \sqrt{Sen \times Spe}$$

$$F1 = \frac{(2 \times Pr \times Sen)}{(Pr+Sen)}; MCC = \frac{TP/N - S \times P}{\sqrt{P \times S \times (1-S) \times (1-P)}}$$

Here, $TP$:True Positive, $TN$:True Negative, $FP$:False Positive, $FN$:False Negative, $N = (TP + TN + FP + FN)$, $P = (TP + FP)/N$, $S = (TP + FN)/N$. Vessel segmentation is a case of highly unbalanced data classification. It classifies image pixels into vessel and non-vessel classes. $Acc$ and $Spe$ give the measure of correctly classified vessel pixels ($TP$) and non-vessel pixels ($TN$), respectively. In such cases of data-imbalance, these measures do not suffice. Correct segmentation of thin vessels pixels, hardly affects the values of $Acc$ and $Spe$, which is mis-leading. The value of $Sen$ increases with the correct extraction of fine vessels and boundary vessel pixels. Thus, a high value of $Sen$ is a good measure for evaluation of complete vessel map extraction. $Pr$ is another measure which tells about the correctness of classified vessel pixels. $MCC$ is a correlation coefficient between output and ground truth. Other measures are mathematical combinations of previous metrics.

Area Under the Receiver Operating Characteristics Curve (AUC-ROC) is a curve between $Sen$ (True Positive Rate) and $1 - Spe$ (False Positive Rate). Ideal ROC is has AUC

TABLE I: Performance comparison of proposed algorithm on DRIVE dataset

| Method | Acc | Sen | Spe | Pr | F1 | G | MCC | AUC |
|---|---|---|---|---|---|---|---|---|
| Al Diri et al. [16] | NA | 0.728 | 0.955 | NA | NA | 0.834 | NA | NA |
| Roychowdhury et al. [15] | 0.952 | 0.725 | 0.983 | NA | NA | 0.844 | NA | 0.962 |
| Azzopardi et al. [3] | 0.944 | 0.765 | 0.970 | NA | NA | 0.861 | 0.747 | 0.961 |
| Soares et al. [11] | 0.947 | 0.728 | 0.979 | NA | NA | 0.844 | NA | 0.961 |
| Liskowski et al. [7] | 0.949 | 0.776 | 0.977 | NA | NA | 0.871 | NA | 0.972 |
| Orlando et al. [9] | NA | 0.790 | 0.968 | 0.785 | 0.786 | 0.874 | 0.756 | 0.951 |
| Yan et al. [2] | 0.954 | 0.765 | 0.982 | NA | NA | 0.867 | NA | 0.975 |
| Alom et al. [5] | 0.956 | 0.779 | 0.981 | NA | 0.817 | 0.874 | NA | 0.978 |
| Jiang et al. [18] | 0.971 | 0.784 | 0.989 | NA | 0.825 | 0.881 | NA | 0.986 |
| **Proposed method** | **0.966** | **0.884** | **0.973** | **0.760** | **0.817** | **0.928** | **0.801** | **0.980** |

TABLE II: Performance comparison of proposed algorithm on STARE dataset

| Method | Acc | Sen | Spe | Pr | F1 | G | MCC | AUC |
|---|---|---|---|---|---|---|---|---|
| Al Diri et al. [16] | NA | 0.752 | 0.968 | NA | NA | 0.853 | NA | NA |
| Roychowdhury et al. [15] | 0.951 | 0.772 | 0.973 | NA | NA | 0.867 | NA | 0.969 |
| Azzopardi et al. [3] | 0.950 | 0.772 | 0.970 | NA | NA | 0.865 | 0.733 | 0.956 |
| Soares et al. [11] | 0.948 | 0.720 | 0.975 | NA | NA | 0.838 | NA | 0.967 |
| Liskowski et al. [7] | 0.957 | 0.787 | 0.975 | NA | NA | 0.876 | NA | 0.978 |
| Orlando et al. [9] | NA | 0.768 | 0.974 | 0.774 | 0.764 | 0.865 | 0.742 | 0.971 |
| Yan et al. [2] | 0.961 | 0.758 | 0.985 | NA | NA | 0.864 | NA | 0.980 |
| Alom et al. [5] | 0.971 | 0.830 | 0.986 | NA | 0.847 | 0.905 | NA | 0.991 |
| Jiang et al. [18] | 0.978 | 0.825 | 0.990 | NA | 0.849 | 0.904 | NA | 0.993 |
| **Proposed method** | **0.958** | **0.896** | **0.963** | **0.680** | **0.775** | **0.929** | **0.762** | **0.982** |

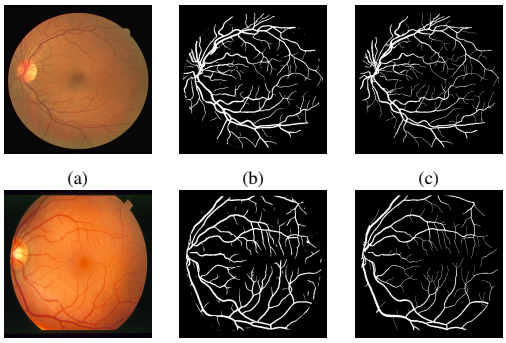

Fig. 7: Illustration of simulation results : (a) Input fundus '01_test' from DRIVE , (b) Output Vessel Map (c) Ground Truth given by Expert-1; (d) Input fundus 'im0077' , (e) Output Vessel Map (f) Ground Truth given by Expert-1

value 1. Fig. 6 shows the mean ROC for DRIVE and STARE data-sets. It shows that the proposed algorithm has performed consistently well on both the data-sets obtaining very nearby $AUC$ values (DRIVE : $0.9804$, STARE : $0.9823$). The small difference of $0.0019$ proves the robustness of algorithm on two different data-sets.

Fig. 7 presents the results of proposed algorithm on two sample fundus images taken from DRIVE and STARE databases. Fig. 7 (a) is the color fundus image '01_test' from DRIVE. Fig. 7 (b) shows the segmented binary vessel map using the given algorithm. Fig 7 (c) gives the corresponding ground truth annotated by Expert-1. Similarly, the next row (Fig. 7 (d), (e) and (f)) shows the images corresponding to image 'im0077' from STARE dataset. These figures clearly show that the proposed method has been quite successful in segmenting complete vessel map which includes fine vessels and boundary pixels of thick vessels.

Table I and II present a comparison of the proposed method with other state-of-the-art methods in terms of all the above-mentioned metrics. It can be seen that the algorithm has performed outstandingly well in terms of $Sen$ which is most affected with the correct segmentation of fine vessels and vessel-boundary pixels. Proposed algorithm has extracted vessels from low-contrast regions too, which leads into extraction of a complete vessel map. Other measures like $AUC$, $G$ and $MCC$ are also better than the other existing methods.

## IV. Conclusion

Segmentation of complete retinal vessel map using fundus images is challenging due to presence of many low-contrast regions where vessels merge into the background. This paper addresses the problem of precise vessel segmentation in poor contrast regions. It handles the background vessel-like texture in a sophisticated manner without harming the vessel pixels. The method presented is novel and it outperforms state-of-the-art methods, specially in terms of sensitivity. The simulation results have shown major improvements in low-contrast regions like fine vessel-endings and vessel-boundary pixels.

## References


[1] Z. Fan, J. Lu, C. Wei, et al., "A hierarchical image matting model for blood vessel segmentation in fundus images," IEEE Trans. Image Process., 28, (5), pp. 2367−2377, 2019.

[2] Z. Yan, X. Yang, and, K. Cheng, "Joint segment-level and pixel-wise losses for deep learning based retinal vessel segmentation," IEEE Trans. Biomed. Eng., 65(9), pp.1912−1923, 2019.

[3] G. Azzopardi, N. Strisciuglio, M. Vento, et al., "Trainable COSFIRE filters for vessel delineation with application to retinal images," Medical image analysis, 19, (1), pp. 46−57, 2015.

[4] O. Ronneberger, P. Fischer, and T. Brox, "U-net: Convolutional networks for biomedical image segmentation," in MICCAI, pp. 234241, 2015.

[5] M. Z. Alom, M. Hasan, C. Yakopcic, et al., "Recurrent residual convolutional neural network based on u-net (R2U-net) for medical image segmentation," arXiv preprint arXiv:1802.06955, 2018.

[6] E. D. Pisano, S. Zong, B. M. Hemminger, et al., "Contrast limited adaptive histogram equalization image processing to improve the detection of simulated spiculations in dense mammograms," Journal Dig. Imaging, 11, (4), pp. 193−200, 1998.

[7] P. Liskowski, and K. Krawiec, "Segmenting retinal blood vessels with deep neural networks," IEEE Trans. Med. Imaging, 35, (11), pp. 2369−2380, 2016.

[8] S. Chaudhuri, S. Chatterjee, N. Katz, et al., "Detection of blood vessels in retinal images using two-dimensional matched filters," *IEEE Trans. Med. Imaging*, vol. 8, no. 3, pp. 263−269, 1989.

[9] J. I. Orlando, E. Prokofyeva, M. B. Blaschko, "A discriminatively trained fully connected conditional random field model for blood vessel segmentation in fundus images," IEEE Trans. Biomed. Eng., 64, (1), pp. 16−27, 2017.

[10] S. Paris, S. W. Hasinoff, and J. Kautz, "Local laplacian filters: Edge-aware image processing with a laplacian pyramid," ACM Trans. Graph., 30, (4), pp. 68, 2011.

[11] J. Soares, J. J. Leandro, R. M. Cesar, et al., "Retinal vessel segmentation using the 2−D Gabor wavelet and supervised classification," IEEE Trans. Med. Imag., 25, (9), pp. 1214−1222, 2006.

[12] A. Hoover, V. Kouznetsova, M. H. Goldbaum, et al., "Locating blood vessels in retinal images by piece-wise threshold probing of a matched filter response," IEEE Trans. Med. Imaging, 19, (3), pp. 203−210, 2000.

[13] M. Niemeijer, J. Staal, B. V. Ginneken, et al., "DRIVE: Digital Retinal Images for Vessel Extraction," 2004. [Online]. Available: http://www.isi.uu.nl/Research/Databases/DRIVE

[14] D. Marín, A. Aquino, M. E. Gegúndez-Arias, et al., "A new supervised method for blood vessel segmentation in retinal images by using gray-level and moment invariants-based features," IEEE Trans. Med. Imaging, 30, (1), pp. 146−158, 2011.

[15] S. Roychowdhury, D. D. Koozekanani, and K. K. Parhi, "Iterative vessel segmentation of fundus images," IEEE Trans. Biomed. Eng., 62, (7), pp. 1738−1749, 2015.

[16] B. Al-Diri, A. Hunter, and D. Steel, "An active contour model for segmenting and measuring retinal vessels," IEEE Trans. on Med. Imaging, 28, (9), pp. 1488−1497, 2009.

[17] K. Upadhyay, M. Agrawal, and P. Vashist, "Unsupervised Multiscale Retinal Blood Vessel Segmentation using Fundus Images," IET Image Processing, 2020.

[18] Y. Jiang, N. Tan, T. Peng, et al., "Retinal Vessels Segmentation Based on Dilated Multi-Scale Convolutional Neural Network," IEEE Access, 7, pp. 76342−76352, 2019.